# Assessment of Sensitivity and Validity Hydrodynamic Model in Cisadane Using Delft3d Flow Model

Gumilang Ramadhan Pasma[1]*, Hamzah Haru Radityo Suharyanto[1], Hanah Khoirunnisa[1], Reni Wijayanti[2], Gugum Gumbira[1,3], Reno Arief Rachman[1]

[1]Research Center for Hydrodynamics Technology, National Research and Innovation Agency
Jl. Hidro Dinamika, Sukolilo, Surabaya, Jawa Timur 60112 Indonesia
[2]Research Center for Oceanography, National Research and Innovation Agency
Jl. Pasir Putih Raya No.1 Jakarta Utara, Daerah Khusus Ibukota Jakarta 14430 Indonesia
[3]Civil and Industrial Engineering Department, University of Liverpool
Liverpool, L69 3GQ United Kingdom
Email: gumilang.ramadhan.pasma@brin.go.id

***Abstract***

*The National Capital Integrated Coastal Development (NCICD) program was prioritized as a disaster reduction technology within the annual target of BRIN in 2022. It is a part of the North Java Coastal Integrated Development Program project. A coastal reservoir development plan at the Cisadane River estuary is one of the outcomes. In this case, hydrodynamic modelling is needed to acquire hydrodynamic properties under the existing condition of Cisadane downstream, and it applied the Delft3D-FLOW model. The bathymetric data used in this simulation was obtained from the assimilation of national bathymetric data with a grid spacing of 180 m and field survey data with a horizontal resolution of 10 m and transect spacing of 200 m seaward of the Cisadane estuary. It has interpolated in a regular structured grid with 100 m and 50 m grid spacing. In addition, other data used are three hourly wind data downloaded from the European Centre for Medium-Range Weather Forecasts (ECMWF) and the daily discharge of the Cisadane River in 2021. Astronomical water level data generated from TPXO 7.2 and TPXO 8 were used in the boundary conditions. These data are simulated using the two and three-dimensional flow model Delft3D-FLOW during November 1 – 15, 2021, using four manning coefficients (n) values, which are 0.03; 0.035; 0.04; and 0.045. The validation formulation used Normalization Root Mean Square Error (NRMSE), resulting in 5.3 - 9.6% for all the manning values and domains. The highest correlation coefficient of current velocity (u-v components) is acquired in the 10 km$^2$ domain with 0.797 for the L3 (bottom layer).*

***Keywords:*** *Delft3D-FLOW, Hydrodynamic, Manning number, Three-dimensional model*

## Introduction

The world's urban area sinking at the fastest rate is Jakarta (Subsidence, 2015). According to Abidin *et al*. (2011), some areas of North Jakarta are sinking at a rate of 15 cm annually, with Muara Baru experiencing the deepest fall of 4.1 m between 1974 and 2010 (Ministry of Public Works, 2011). Since 2013, the governments of Indonesia and the Netherlands have been working together on the National Capital Coastal Integrated Development Program (NCICD) (Octavianti and Charles, 2018). The NCICD is part of the National Strategic Program in the National Medium-Term Development Plan 2020-2024 (BPPT, 2020). The program is included in the main strategic priority project number 27, namely Coastal Security 5: Urban North Coast of Java (Presidential Regulation No. 18 of 2020). One of the next steps taken is planning to construct a Coastal Reservoir, which is proposed as a holistic and sustainable solution to the emerging problems in Jakarta Bay. In the proposed coastal reservoir concept, a construction project is envisaged to establish a 50.6 km embankment, positioned at a depth of -20 m, extending from Cisadane Estuary in the Banten Province to Gembong Estuary in the West Java Province (Wibowo *et al*., 2022). BAPPENAS, the responsible authority, intends to develop a pilot plan for the coastal reservoir along the Cisadane Estuary, taking into consideration the sedimentation patterns and methods prevalent in the Cisadane Estuary (Wibowo *et al*., 2022). Consequently, a comprehensive investigation of the hydrodynamic analysis of the current state in the vicinity of the Cisadane River, which will serve as essential information for the effective design, construction, and operation of the coastal reservoir and it will be underpinned by the acquisition and analysis of various field data.

Sea level and river discharge affect tidal dynamics and inundation areas in Jakarta Bay. This research was carried out by Surya *et al*. (2019) using

*) Corresponding author

https://ejournal.undip.ac.id/index.php/ijms
DOI: 10.14710/ik.ijms.29.1.133-146
Received : 02-11-2023
Accepted : 27-01-2024

the finite volume coast model (FVCOM). Hydrodynamic modelling using MIKE 21 and Delft3D has been carried out in the Jakarta Bay area, and it is found that reclamation has no significant effect on current patterns (Jasmin *et al*., 2019; Ihsan, 2020; Nugroho and Magdalena, 2020).

Delft3D software is capable of simulating coastal hydrodynamic processes by using its FLOW module. FLOW module includes two hydraulic parameters: bed roughness and viscosity (Deltares, 2022). The simulation's overall sensitivity depends on each parameter's value range. Several studies focus on testing the range of parameters that affect the FLOW module run. A study by Brakenhoff *et al*. (2020) found that a higher roughness parameter induces a lower current velocity in Delft3D-FLOW. Common finding shows that the flow direction of the current velocity stayed the same when the adjusted roughness parameter was applied in the model. Typically, roughness at a smooth surfaced seafloor is ruled by the skin friction from individual grains related to assumed uniform bed composition. From a hydrodynamic perspective, the intensity and directional components of currents resulting from tidal and wave forces are influenced by the induced bed friction, which is characterized by a roughness parameter assumed to calibrate the hydrodynamic model. It is worth noting that the roughness parameterization directly impacts the magnitude of sediment transport that occurs subsequently (Brakenhoff *et al*., 2020; Khanarmuei *et al*., 2020).

In coastal settings, previous studies have shown that Manning's roughness approximation is suitable for simulating related hydraulic losses due to bed conditions. Moreover, any change in this parameter affects overall model sensitivity (Briere *et al*., 2011; Mayo *et al*., 2014; and Holt *et al*., 2015). Bao *et al*. (2009) and Cea and French (2012) stated that using proper bottom friction parameter value in the hydraulic-hydrodynamic models minimizes simulation errors. Furthermore, Bastidas *et al*. (2016) also revealed that the Manning coefficient has higher sensitivity in the region where the tidal amplitude is high with shallow depth. Delft3D-FLOW module uses Manning's roughness values to be converted into a depth-dependent Chézy roughness in a typical computational scheme (Deltares, 2022). Hydrodynamic model assessment in Sunda Strait has been studied using Delft3D (Pratama *et al*., 2020).

Previous research has been carried out by comparing hydrodynamic models in Western Port Bay, Australia using MIKE 21 FM, DELFT3D and DELFT3D FM (Symonds *et al*., 2016). An unstructured grid was utilized in MIKE21 FM and Delft3D FM modeling, while a structured grid was used in Delft3D modeling. Computational efficiency comparison shows that DELFT 3D has the best result when using a single core (18 h run time, 0.81 sec.cell efficiency$^{-1}$). In comparison, MIKE21 FM has better results when used with multiple cores (12 h run time, 0.43 sec/cell efficiency using eight cores). On the other hand, water level and current conditions indicate that Delft3D has results closer to the actual data than MIKE21 FM and DELFT 3D FM (Symonds *et al*., 2016). Another model is used by comparing with the PISCES model which states that the current velocity of the DELFT3D modelling results at various stations shows better results for validation (Walstra *et al*., 2001). Based on extensive review studies, it has been established that Delft3D exhibits better performance than other models. Consequently, the objective of this study is to assess the sensitivity of the Delft3D model to variations in the Manning number, boundary conditions, and model extent. This study will be accomplished by validating water level and current speed and direction simulations using field data.

## Materials and Methods

### *Study site*

The study site is located in the waters of Tanjung Pasir, Tangerang, Banten, near the mouth of the Cisadane River. Figure 1 illustrates the coverage of the study area along with the corresponding detailed data. This location is of significant importance as it will serve as the primary focus area for the National Capital Integrated Coastal Development (NCICD) project.

### *Data source*

The input data used are primary and secondary data obtained from several sources, National Bathymetry data BatNas v1.5 with a resolution of 180 m x 180 m for the Cisadane water area and its surroundings (BIG, 2021). The data are assimilated with data from primary data hydrographic surveys taken on November 1 - 14, 2021. In addition, this modeling also used wind data from the European Center Medium Weather Forecast (ECMWF) at coordinates of 106.6$^{o}$ E and -5.6$^{o}$ S with a data interval of 3 hours for 15 days (Molteni *et al*., 1996).

A daily average Cisadane River discharge data for 15 d from the 2015-2020 data of the Ciliwung-Cisadane River Basin Organization is also used as input for this simulation. The boundary condition data in this model are astronomical tide data from TPXO 7.2 and TPXO 8 obtained through the Delft dashboard (Ormondt *et al*., 2020). The TPXO 8 is the newest version of the tide model with a finer geographical grid (1/6-degree resolution grid) than the previous version (1/4-degree) (Rautenbacht *et*

*al*., 2019 and OSU, 2023). Hydrodynamic modeling and comparison between Tidal Model Driver (TMD) data to TPXO 7.2 were carried out by Wahyudi *et al*. (2019) and obtained correlation results of r = 0.9996. Verification of the model results against field data around the Cisadane River obtained on November 1-14, 2021 (BTIPDP, 2021). The data includes the magnitude and direction of the currents and free surface elevations.

### *Model description*

The model used in this study is the Delft3D-FLOW Hydrodynamics model, a software developed by Deltares. Delft3D-FLOW is a program that can run two- and three-dimensional hydrodynamic simulations using rectilinear or curvilinear grids (Deltares, 2022). In this study, a rectilinear grid with two sizes (50 m x 50 m and 100 m x 100 m) was applied. The governing equation used in this Delft3D-FLOW modeling is a three-dimensional Navier-Stokes equation that is derived explicitly for shallow water, as formulated in equation (1) as referred to Delft3D manual by Deltares, 2022:

$$\frac{\partial u_i}{\partial t} + u_i \frac{\partial u_j}{\partial x_i} + \frac{1}{\rho_0}\frac{\partial p}{\partial x_i} - \frac{1}{\rho_0}\frac{\partial \tau_{ij}}{\partial x_j} + \varepsilon_{ijk} 2\Omega_j u_k = \frac{\rho}{\rho_0} g \delta_{i3} \quad (1)$$

where $\delta_{ij}$ is the Kronecker delta, $\varepsilon_{ijk}$ is the permutation symbol, $\Omega_j$ is the planetary vorticity and $\tau_{ij}$ is the turbulent stresses, while $p$ is a hydrostatic and hydrodynamic pressure. Based on the Navier-stokes equation in shallow water, it can be derived into a momentum and continuity equations as below:

$$\frac{\partial u}{\partial t} + \frac{1}{\rho_0}\frac{\partial p}{\partial x}\int_z^\zeta p g dz' + \frac{1}{\rho_0}\frac{\partial q}{\partial x} = RHS_x \quad (2)$$

$$\frac{\partial v}{\partial t} + \frac{1}{\rho_0}\frac{\partial p}{\partial y}\int_z^\zeta p g dz' + \frac{1}{\rho_0}\frac{\partial q}{\partial y} = RHS_y \quad (3)$$

$$\frac{\partial w}{\partial t} + \frac{1}{\rho_0}\frac{\partial q}{\partial z} = RHS_z \quad (4)$$

Moreover, the continuity equation is defined as:

$$\frac{\partial u_i}{\partial x_i} = 0 \quad (5)$$

### *Model scheme*

With case studies surrounding the Cisadane River, this simulation attempts to assess the sensitivity of the hydrodynamic model utilizing Delft 3D FLOW to three parameters: model extent and grid size, bed roughness, and the type of boundary condition. This simulation uses two grid sizes, 50 m x 50 m and 100 m x 100 m, and four model extents, 10km$^2$, 20km$^2$, 25km$^2$, and 30km$^2$ correspondingly (Figure 2b.). Four manning number values are used for each model extent scenario: 0.03; 0.035; 0.04; and 0.045 (Figure 2a.). The selection of these four combinations is predicated upon considering the available computational resources and the quantity of cells below 5000.

Furthermore, the accuracy of the hydrodynamic modeling outcomes will be evaluated within regions characterized by the most refined grid specifications. Additionally, TPXO 7.2 and TPXO 8.0 boundary conditions are applied in each simulation. There are 64 trials for the two-dimensional simulation, with each boundary condition applied to every scenario. This model was performed in 2D and 3D to get the optimal hydrodynamic modeling configuration

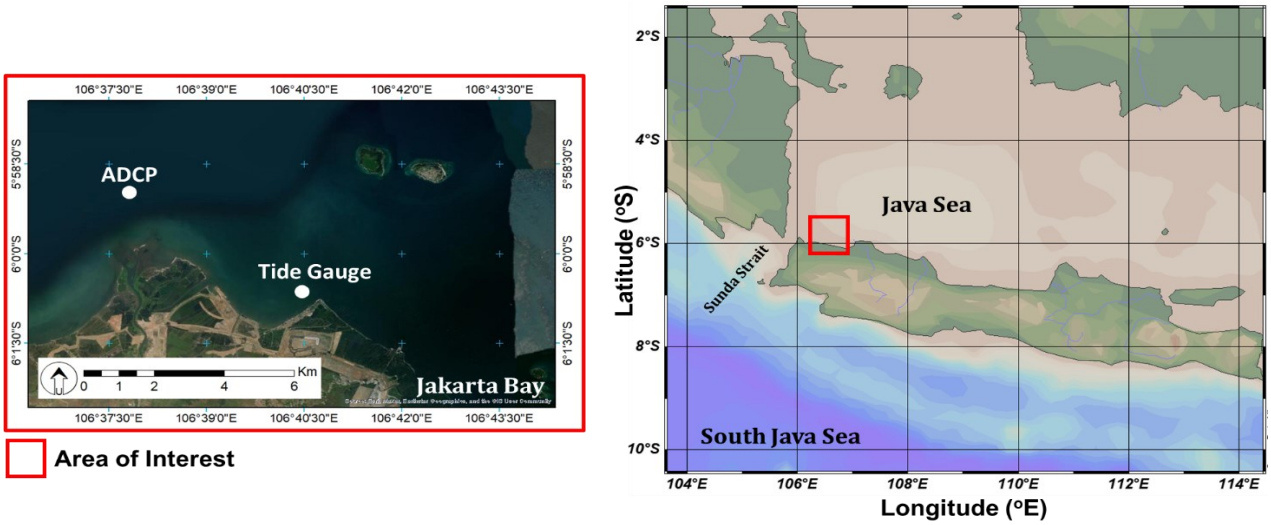


**Figure 1.** The location of field survey data point of ADCP and tide gauge point.

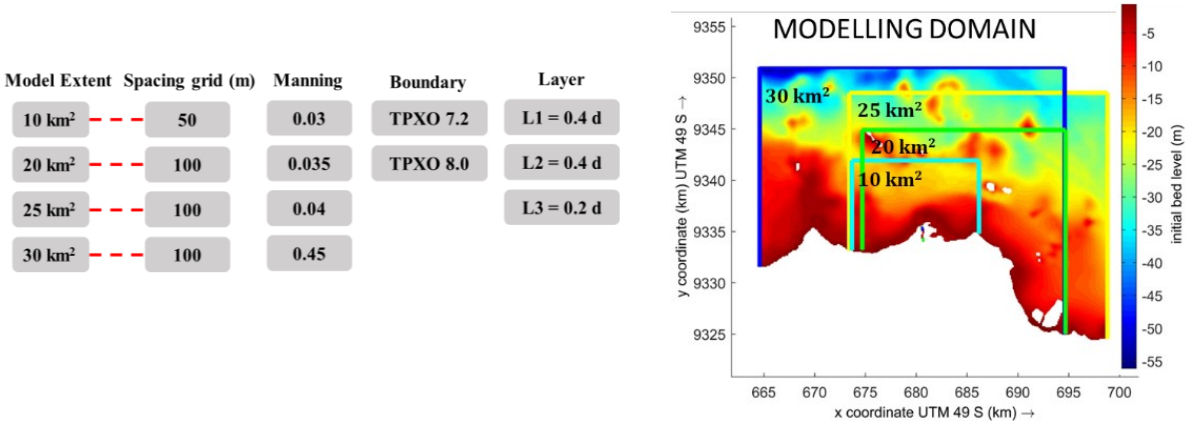


**Figure 2.** (a) Model scenario and model sensitivity concept, (b) modelling domain.

near the Cisadane River. For 3D simulation, the manning number value with the best validation outcomes for each domain will be applied.

### *Model validation*

This study employs three validation and accuracy calculations. Firstly, it involves the comparison of water levels obtained from the 2D model with tidal data collected at the coordinates -6.019432°S and 106.669673°E in the vicinity of the Cisadane River, utilizing the Root Mean Square Error (RMSE), Normalization Root Mean Square Error (NRMSE), and Skill formula (Williams and Esteves, 2017). The last validation was carried out by comparing the value of the east-west velocity vectors to the current velocity data of the Acoustic Doppler current profiler (ADCP) at coordinates -5.988324°S and 106.630840°E (Figure 2.) using the correlation equation (Williams and Esteves, 2017). East-west current velocity is obtained through a three-dimensional model flow, where it was divided into three layers, which were L1 (surface), L2 (middle), and L3 (bottom). In further examination, all those layers will be observed towards influence of Manning's number difference.

$$RMSE = \sqrt{\frac{\sum_{t=1}^{T}(X_{model} - X_{obs})^2}{T}} \quad (6)$$

$$NRMSE = \frac{RMSE}{X_{max} - X_{min}} \quad (7)$$

$$Skill = 1 - \frac{\sum|X_{model} - X_{obs}|^2}{\sum(|X_{model} - \overline{X_{obs}}| + |X_{obs} - \overline{X_{obs}}|)^2} \quad (8)$$

Based on equations 6 and 8 $X_{model}$ is a result of the hydrodynamic model and $X_{obs}$ is a field tide gauge data. The free surface elevation model data are compared against tidal data from the tide gauge (field observation) using the RMSE and NRMSE formula (Equations 6 and 7). Scatter plots and correlation statistics have proven valuable tools for assessing the concurrence between measured and modeled data in the context of multidirectional sea states (Williams and Esteves, 2017).

$$R = \frac{\sum_{i=1}^{N_i}(S_i - \overline{S_i})(O_i - \overline{O_i})}{\sqrt{\sum_{i=1}^{N_i}(S_i - \overline{S_i})^2}\sqrt{\sum_{i=1}^{N_i}(O_i - \overline{O_i})^2}} \quad (9)$$

Consequently, the present study adopts correlation analysis to augment the accuracy of results within the three-dimensional model, employing based on Equation 9. The value of $R$ is the level of correlation of two data with a value of 0 to 1, where if the value of $R$ is close to 1, the data has a high degree of connectedness (Williams and Esteves, 2017). In addition, $S_i$ is the model result data and $O_i$ is the field current velocity data. The free surface elevation model data are compared against tidal data from the tide gauge (field observation) using the RMSE, NRMSE, and Skill formula (Equations 6, 7, and 8). A similar validation approach has been made by Warner *et al*. (2005), Williams and Esteves (2017) and Khoirunnisa *et al*. (2021).

## Result and Discussion

This study investigated the three primary hydrodynamic modelling parameters (domain and grid size, manning number, and boundary condition) to determine the best configuration. Comparing the grid size and model extent comes first in this test, followed by comparing the bed roughness and boundary condition values. The optimum configuration based on two-dimensional simulation will also be utilised for three-dimensional hydrodynamic simulation to reach the impact of bed roughness values on L1, L2, and L3.

### *Comparison of model extent and grid size*

The skill range varies in a similar pattern for all domains; as we can see in 10 km$^2$ domain, the index of agreement (skill) range is 0.975 to 0.988, while the 20 km$^2$ domain is 0.965 to 0.987 next one, the 25 km$^2$ domain is 0.976 to 0.987, and the last is the 30 km$^2$ domain in the 0.971 to 0.987 range. Surya *et al*., (2019) proposed a statistical method for assessing model skill in the context of verification. This skill represents the degree of divergence between prediction and observation data. A skill assessment of 1.00 indicates complete agreement between model data and observation data.

From a statistical standpoint, it is observed that the error values across all scenarios range from 0.057 to 0.095 m in the direction towards the primary data, with a tidal range about 1.08 m. This indicates that the trend of error in the model outputs remains below 0.1 m when compared to the field data. The best accuracy calculation combination is obtained in a domain with an area of 10 km$^2$ with a value range of RMSE 0.05795 m to 0.08156 m, Skill 0.97548 to 0.988174, and NRMSE 5.34% to 7.512%. The difference between measured and modelled data is expressed as accuracy. A minimum of 10% difference between the model and actual data is ideal. The root mean square error (RMSE) statistic can also be used to quantify the accuracy of the modelled data.

The RMSE number is frequently given as a percentage, with lower values indicating less residual variance and improved model performance (Williams and Esteves, 2017). Overall, the model is good enough to simulate the actual condition. Hence, a smaller grid size indicating high spatial resolution and a grid size of 50 m (10 km$^2$ domain) produces better results than other grid sizes. This condition is also achieved by Parsapour-moghaddam *et al*. (2018).

Model extent and bathymetry rule the numerical stability of the model. As we can conclude from Figure 2b and Table 1, the domain for 20 km$^2$ and 30 km$^2$ has shown an unstable model run in several Manning values. It can be caused by the bathymetry condition in the edge of the model domain, where the bounding box coincides with several patches of shallow depth. After a thorough model check, this condition of bathymetry has caused an unstable/jet-like current induced by the TPXO water level boundary condition, as also agreed by Nuraghnia *et al*. (2021).

### *Comparison of bed roughness*

The Manning number (n) values employed in this study as a representation of bed roughness are 0.03; 0.035; 0.040; and 0.045, respectively. Each manning number is examined in two-dimensional (2D) modeling for all domain regions (10km$^2$, 20km$^2$, 25km$^2$, and 30km$^2$, respectively) and two different kinds of boundary conditions (TPXO 7.2 and TPXO 8.0). The two-dimensional hydrodynamic model underwent 64 experiments in all. The manning number 0.045 displays the most optimum simulation outcomes for all model extent and grid size scenarios, according to the results of the two-dimensional hydrodynamic simulation (Table 1.).

Given the relatively negligible disparity observed in water level validation, a thorough analysis of current velocity within the 3D model is conducted primarily to elucidate the impact of bed roughness, which is expected to be more pronounced in the 3D model, particularly within the bottom layer. For all domains and grid sizes, the manning number of 0.03 has the lowest validation value, followed by 0.035 and 0.04. In the Sunda Strait study area, other models had the best manning number value of 0.024 (Pratama *et al*., 2020). There are several scenarios with abnormal results for the 30 km$^2$ domain at 1) manning 0.03 using both TPXO 7.2 and TPXO 8.0 tidal data, 2) manning 0.035 using TPXO 8.0 tidal data, and 3) manning 0.045 using TPXO 7.2 tidal data.

### *Comparison of Boundary Condition*

The differences in the water level graph with different manning in all domains (10km$^2$, 20km$^2$, 25km$^2$, and 30km$^2$, respectively) using TPXO 7.2 and TPXO 8.0 (Figure 3-6). In a thorough comparison, the variation of tidal input data (TPXO 7.2 and TPXO 8.0) and the manning sensitivity (0.03, 0.035, 0.040, 0.045) does not change the flood phase and ebb phase patterns. Both graphs still show the same pattern in the same range of around 0.58 m for maximum high tide and -0.46 m for minimum low tide. However, better results are produced when using the input boundary conditions of TPXO 8.0 (Table 1.) (Rautenbach *et al*., 2019).

The higher manning value shows a smaller deviation (Table 1.). Based on Table 1, TPXO 8.0 has a better validation than TPXO 7.2. This is related to the finer geographical grid (1/6-degree resolution grid) of TPXO 8.0 than TPXO 7.2 (1/4 degree) (Rautenbacht *et al*., 2019 and OSU, 2023). Hence, a smaller grid size indicating high spatial resolution, a grid size of 50 m (10 km$^2$ domain), produces best results than other grid sizes (Figure 4.). This condition is also achieved by Parsapour-moghaddam *et al*. (2018). Based on the validation results of TPXO 8.0, which is higher than TPXO 7.2, the 3D model uses TPXO 8.0 as the input boundary condition.

No substantial variation is observed across the entire model domain in relation to the river boundary. Therefore, it can be concluded that the effect is

negligible due to employing a hydrodynamic-only modeling scheme. A study by Surya *et al*. (2019) demonstrates that the influence of river discharge affects the tidal component solely at the river mouth, while the overall study area remains unaffected by this river discharge. However, it should be noted that this boundary may exhibit significant alterations if a sediment module is incorporated into future studies.

**Table 1**. Comparison of Root Mean Square Error (RMSE) and Model Skill Assessment (SKILL) between the tidal data and water level of Delft3D Flow for manning 0.03, 0.035, 0.04, and 0.045 and TPXO 7.2 and TPXO 8.0.

| Domain (km²) | Manning | 0.03 | | 0.035 | | 0.04 | | 0.045 | |
|---|---|---|---|---|---|---|---|---|---|
| | Boundary data | TPXO 7.2 | TPXO 8 | TPXO 7.2 | TPXO 8 | TPXO 7.2 | TPXO 8 | TPXO 7.2 | TPXO 8 |
| 10 | RMSE (m) | 0.08156 | 0.05804 | 0.08139 | 0.05798 | 0.08133 | 0.05796 | 0.08128 | 0.05795 |
| | NRMSE (%) | 7.512 | 5.346 | 7.49 | 5.34 | 7.49 | 5.338 | 7.49 | 5.336 |
| | Skill | 0.97548 | 0.98813 | 0.97558 | 0.98816 | 0.97562 | 0.988168 | 0.97565 | 0.988174 |
| 20 | RMSE (m) | 0.09548 | 0.06257 | 0.08084 | 0.05943 | 0.08086 | 0.06009 | 0.08088 | 0.06008 |
| | NRMSE (%) | 9.6 | 6.24 | 8.05 | 5.87 | 8.06 | 5.93 | 8.06 | 5.93 |
| | Skill | 0.96580 | 0.98622 | 0.89928 | 0.98783 | 0.97597 | 0.98756 | 0.97595 | 0.98757 |
| 25 | RMSE (m) | 0.07939 | 0.05951 | 0.07930 | 0.05941 | 0.07925 | 0.05941 | 0.07922 | 0.05941 |
| | NRMSE (%) | 7.802 | 5.771 | 7.797 | 5.764 | 7.793 | 5.763 | 7.791 | 5.762 |
| | Skill | 0.97678 | 0.98737 | 0.97684 | 0.98741 | 0.97687 | 0.98741 | 0.97689 | 0.98742 |
| 30 | RMSE (m) | - | - | 0.08719 | - | 0.07017 | 0.05834 | - | 0.05818 |
| | NRMSE (%) | - | - | 8.03 | - | 6.46 | 5.37 | - | 5.36 |
| | Skill | - | - | 0.97124 | - | 0.98188 | 0.98785 | - | 0.98792 |

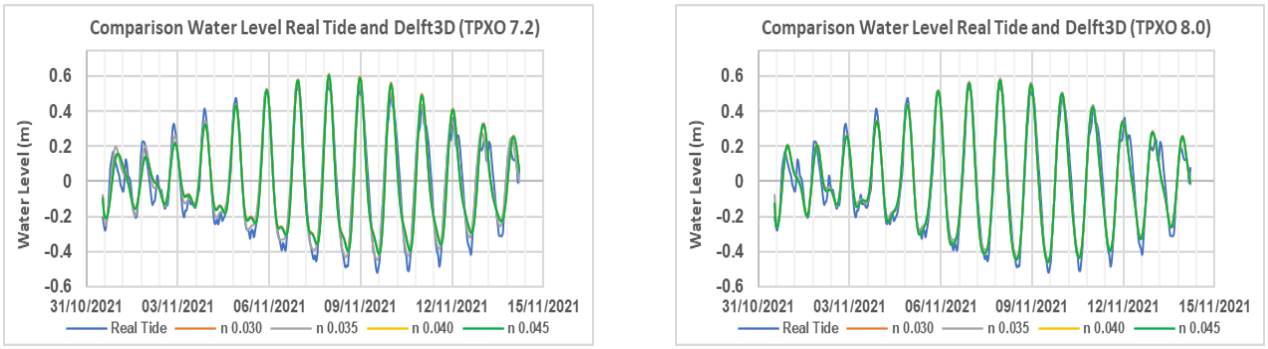


**Figure 3.** Comparison of tidal data from tide gauge and 10km² model scenario using TPXO 7.2 (left) and using TPXO 8.0 (right).

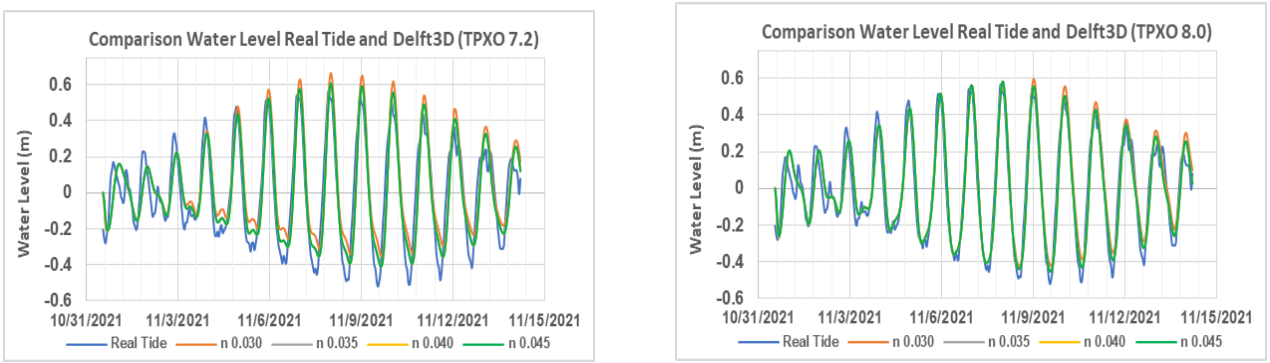


**Figure 4.** Comparison of tidal data from tide gauge and 20km² model scenario using TPXO 7.2 (left) and using TPXO 8.0 (right).

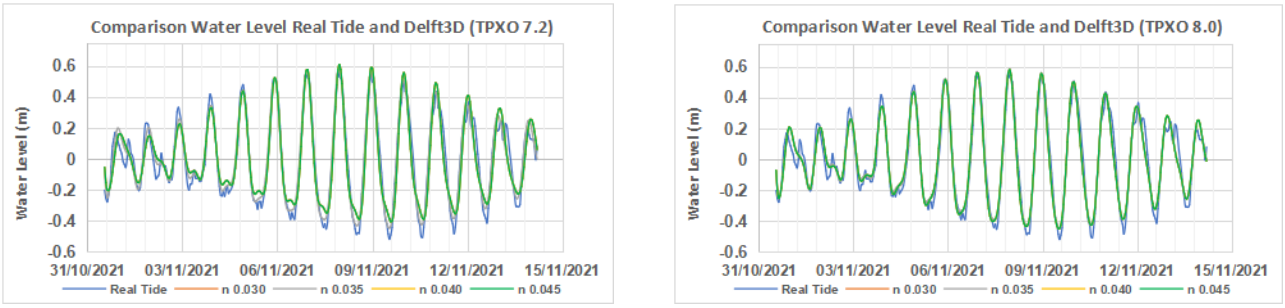


**Figure 5.** Comparison of tidal data from tide gauge and 25km$^2$ model scenario using TPXO 7.2 (left) and using TPXO 8.0 (right).

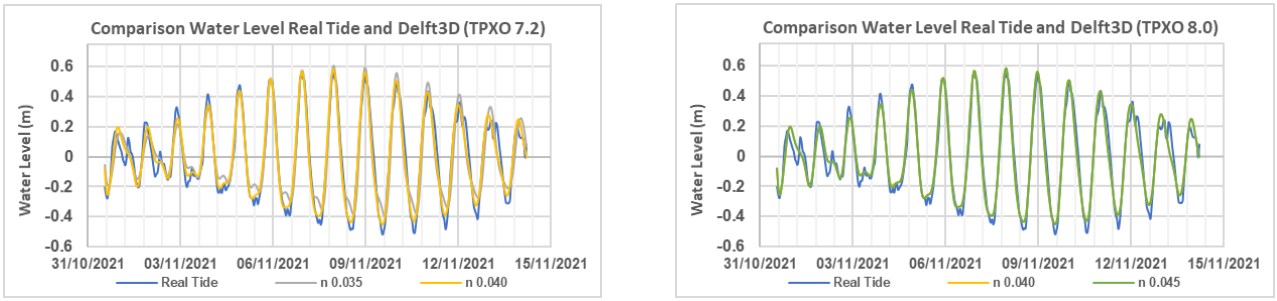


**Figure 6.** Comparison of tidal data from tide gauge and 30km$^2$ model scenario using TPXO 7.2 (left) and using TPXO 8.0 (right).

### *Variations of tidal current*

Under neap and spring tidal conditions, two-dimensional current pattern modeling is conducted. The condition of the tidal current pattern throughout spring and neap is depicted in Figures 7 and 8. According to the spatial analysis, the average current speed during spring has a value range of 0.02 to 0.079 ms$^{-1}$. This value exceeds the velocity condition at neap at this time (0.021 to 0.035 ms$^{-1}$). According to studies by Koh *et al*. (2006), the mean current velocity was around twice as high at spring tide (12± 5 cm s$^{-1}$) as it was at neap (7±4 cm s$^{-1}$) tide.

The present velocity circumstances during neap and spring at the ADCP field observation station are shown in Figure 9 as a verification. A two-dimensional model with a domain size of 10 km$^2$ and a manning number value of 0.045 produced the graph Figures 3, 7, and 9. Neap tide conditions, where the high and low tide amplitude values occur between November 1-3, 2021, and spring tide conditions, where they occur between January 7-11, 2021. Spring and neap conditions is dominantly influenced by interaction of $S_2$ and $M_2$ components (Hussein *et al.,* 2010). The current velocity value at the ADCP observation site has a value range of 0 - 0.25 ms$^{-1}$, according to the graph in Figure 9.

Table 3 reveals that the 10 km$^2$ domain consistently exhibits the highest correlation values across all layers (L1, L2, and L3), and its condition is applied the Manning's number formation in related an advancement further research (n=0,03; n=0,035; n=0,04; and n=0,045). This observation may be attributed to the implementation of a smaller grid size compared to other domains. Similar findings were reported by Warner *et al*. (2005), who demonstrated that finer resolution yielded improved skill values in calculating average current speed.

### *Three-dimensional flow model*

Table 3 shows the correlation values between the Delft3D Flow result against the field current velocity data in each layer for various manning number values. The vertical profile of flow fields produced by the model are compared with the ADCP data as can be seen from Figure 10 to Figure 13. Those figures illustrate the velocity data which is resulted from the optimum Manning's number scenario, domain 10 km$^2$ (n=0.035), domain 20 km$^2$ (n=0.04), domain 25 km$^2$ (n=0.03), and domain 30 km$^2$ (n=0.04), respectively (Table 3.).

The velocity fields present the current magnitudes and directions of the model (orange) and measurement (blue). The model was able to reproduce the flow direction accurately, but underestimated the flow field magnitude. The absence of wave-driven currents is probably the reason behind this. Since the inclusion of wind data in this simulation as wind-induced currents are less dominant, the wave effect on currents is more appropriate in the nearshore region. Meanwhile, Figures 14 to 17 illustrate current speed condition

(magnitude) of all domains in regard of the optimum correlation in all Manning's number, which are domain 10 km$^2$ (n=0.035), domain 20 km$^2$ (n=0.04), domain 25 km$^2$ (n=0.03), and domain 30 km$^2$ (n=0.04), respectively (Table 3). According to Table 3, domain 30 km$^2$ as the largest one has lowest correlation value in all layers (L1, L2, and L3).

Based on the RMSE and Skill calculation for the current speed calculations results for each layer in the 10 km$^2$ area and 0.035 manning, L3 had the lowest RMSE value, 0.088 m, while L2 and L1 had 0.108 m and 0.121 m, respectively. The skill calculations for current speed yielded values of 0.691 at L3, 0.691 at L2, and 0.644 at L1, respectively. Consequently, L3 has the best accuracy with RMSE and Skill combination. According to the model setup, L3 has a layer thickness that is 20% of the overall depth, which is more accurate than L2 and L1. The bed roughness directly impacts the calculation of L3, making it most comparable to the actual field circumstances. One parameterized variable is bedform-related hydraulic roughness, which directly influences the magnitude of friction between the bed and the flowing water (Brakenhoff *et al.,* 2020).

**Table 2.** The average, maximum, and minimum current speed at eight tidal cycles. The gray highlight indicates the highest current speed in the entire cycle.

| Tidal Conditions | | Time | Current speed (ms$^{-1}$) | | |
|---|---|---|---|---|---|
| | | | Average | Maximum | Minimum |
| Neap | Flood Tide | 01/11/2021 12:00 | 0.0354 | 0.9684 | 0.0002 |
| | Flood to ebb tide | 01/11/2021 16:00 | 0.0264 | 0.9772 | 0.0004 |
| | Ebb Tide | 01/11/2021 06:00 | 0.0223 | 0.9874 | 0.0002 |
| | Ebb to flood tide | 01/11/2021 08:00 | 0.0215 | 1.0361 | 0.0002 |
| Spring | Flood Tide | 07/11/2021 13:00 | 0.0207 | 0.9100 | 0.0003 |
| | Flood to ebb tide | 07/11/2021 21:00 | 0.0797 | 0.9520 | 0.0000 |
| | Ebb Tide | 10/11/2021 11:00 | 0.0281 | 0.4680 | 0.0004 |
| | Ebb to flood tide | 07/11/2021 09:00 | 0.0260 | 0.8607 | 0.0002 |

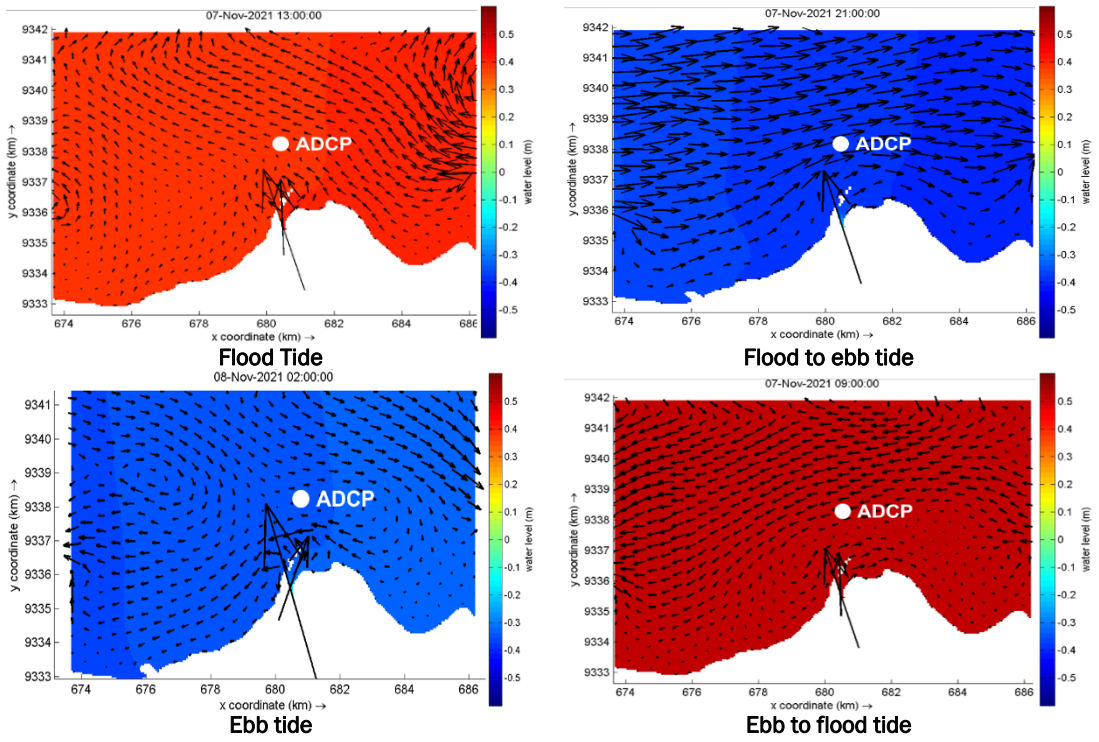


**Figure 7.** The spatial circumstance of current speed and direction in domain size 10 km$^2$ and manning number 0,045. These simulations are plotted at spring and 4 (four) tidal cycles, which are a) flood tide, b) flood to ebb tide, c) ebb tide, and d) ebb to flood tide

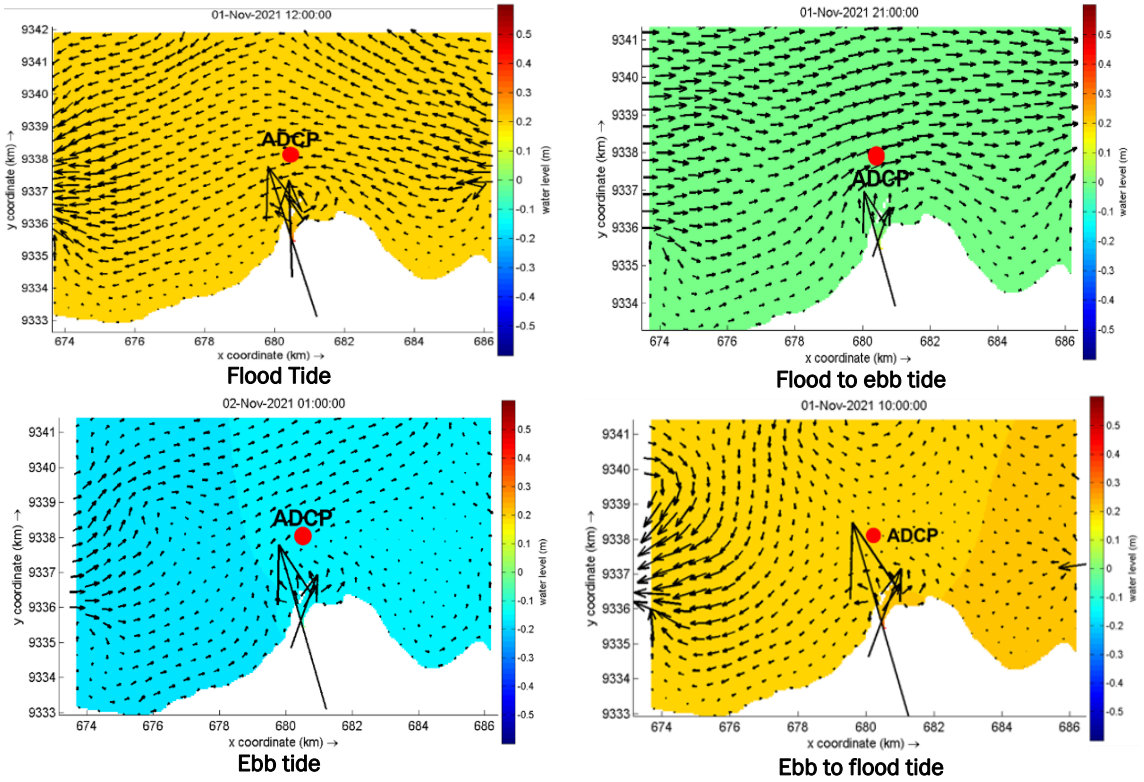


**Figure 8.** Spatial circumstance of current speed and direction in domain size 10 km² and manning number 0,045. These simulations are plotted at neap and 4 (four) tidal cycles, which are a) flood tide, b) flood to ebb tide, c) ebb tide, and d) ebb to flood tide

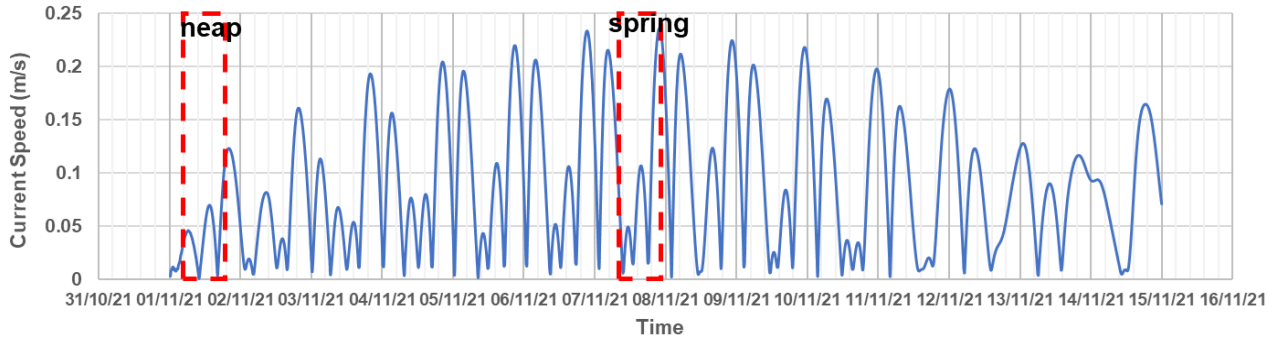


**Figure 9.** The current speed time series profile results from a two-dimensional hydrodynamic simulation at ADCP point with manning number 0.045 and domain size 10 km².

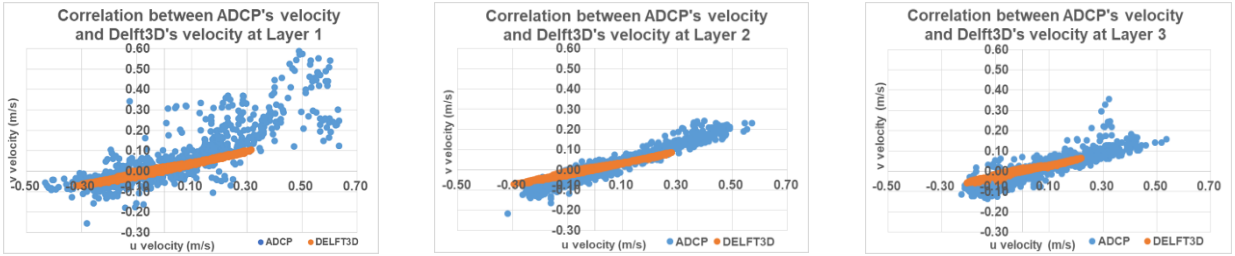


**Figure 10.** Vertical profile of model and ADCP flow fields at domain 10 km² for the highest correlation manning value in Layer 3 (left), Layer 2 (middle), and Layer 1 (right).

**Table 3.** The correlation value of current velocity (u-v components) between the Delft3D Flow model data results and ADCP data in each depth layer with various manning numbers.

| Domain (km²) | Layer | Manning Number | | | |
|---|---|---|---|---|---|
| | | 0.03 | 0.035 | 0.04 | 0.045 |
| 10 | L1 | 0.173 | 0.733 | 0.702 | 0.674 |
| | L2 | 0.261 | 0.797 | 0.764 | 0.717 |
| | L3 | 0.287 | 0.797 | 0.775 | 0.713 |
| 20 | L1 | - | - | 0.671 | 0.637 |
| | L2 | - | - | 0.7294 | 0.699 |
| | L3 | - | - | 0.741 | 0.716 |
| 25 | L1 | 0.691 | 0.653 | 0.613 | 0.574 |
| | L2 | 0.756 | 0.716 | 0.6737 | 0.633 |
| | L3 | 0.751 | 0.722 | 0.690 | 0.659 |
| 30 | L1 | - | - | 0.5489 | 0.5455 |
| | L2 | - | - | 0.5998 | 0.5968 |
| | L3 | - | - | 0.6107 | 0.608 |

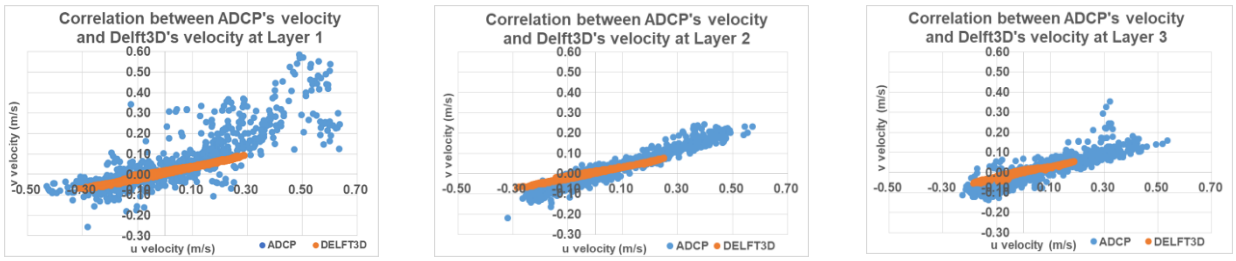


**Figure 11.** Vertical profile of model and ADCP flow fields at domain 20 km² for the highest correlation manning value in Layer 3 (left), Layer 2 (middle), and Layer 1 (right).

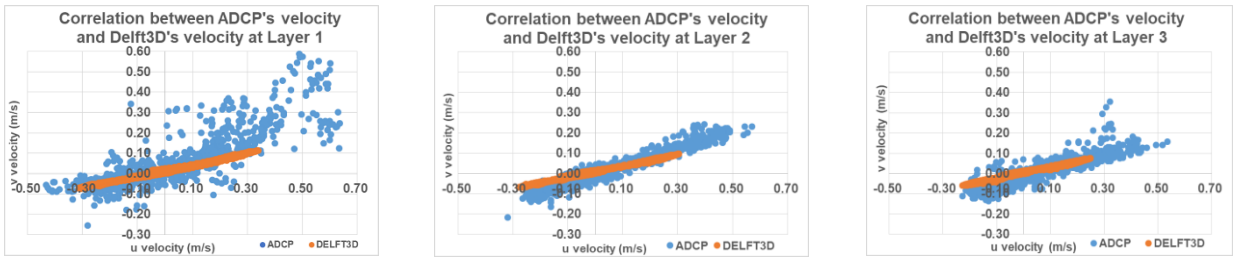


**Figure 12.** Vertical profile of model and ADCP flow fields at domain 25 km² for the highest correlation manning value in Layer 3 (left), Layer 2 (middle), and Layer 1 (right).

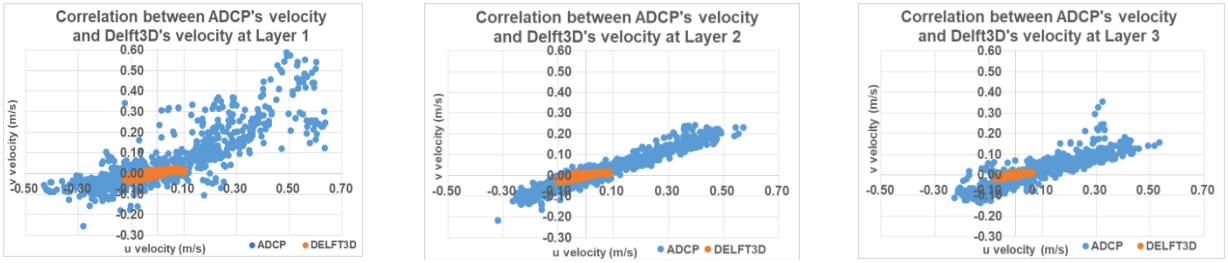


**Figure 13.** Vertical profile of model and ADCP flow fields at domain 30 km² for the highest correlation manning value in Layer 3 (left), Layer 2 (middle), and Layer 1 (right).

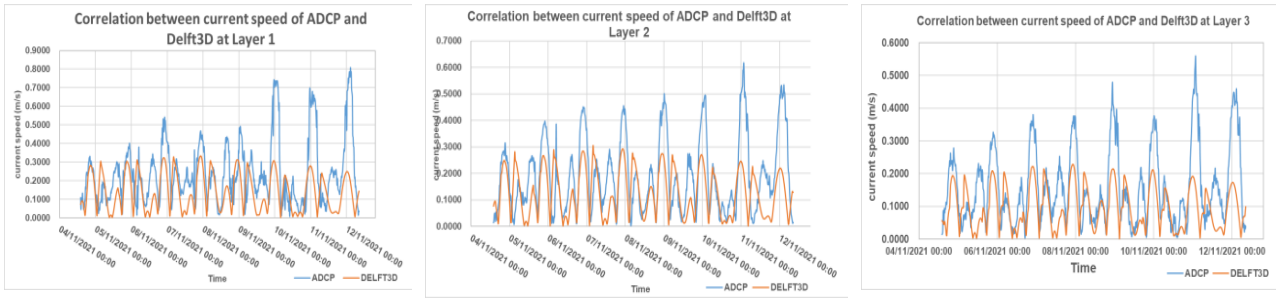


**Figure 14.** Comparison between current speed of ADCP and model on a 10km$^2$ domain.

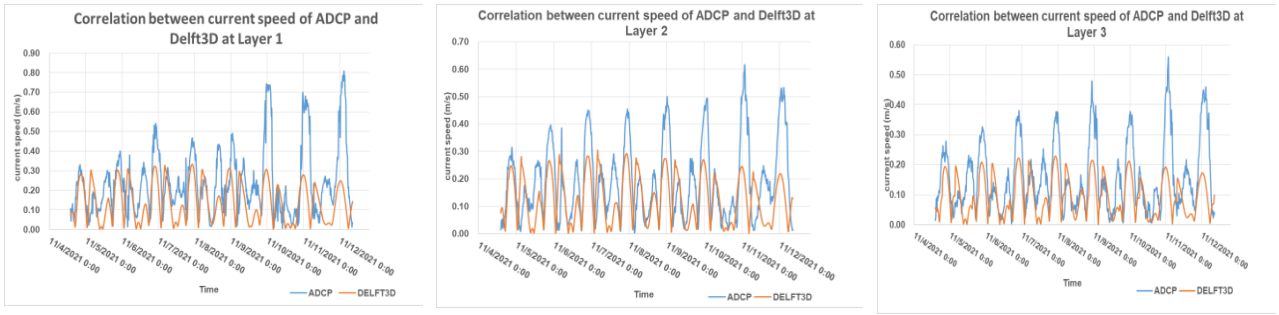


**Figure 15.** Comparison between current speed of ADCP and model on a 20km$^2$ domain.

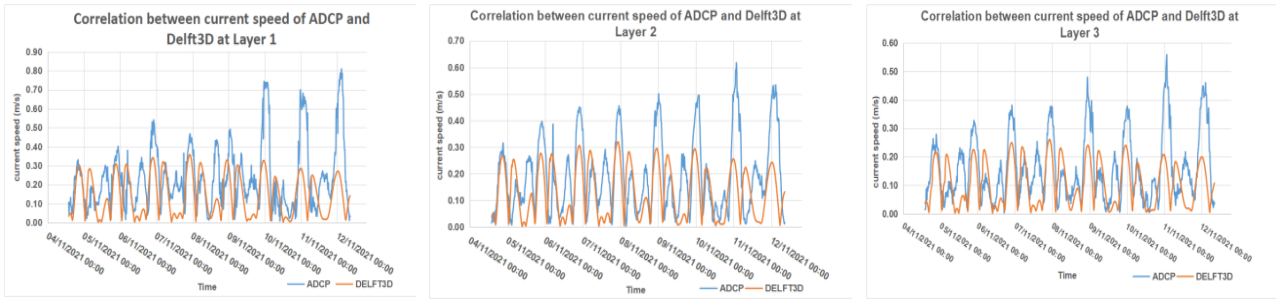


**Figure 16.** Comparison between current speed of ADCP and model on a 25km$^2$ domain.

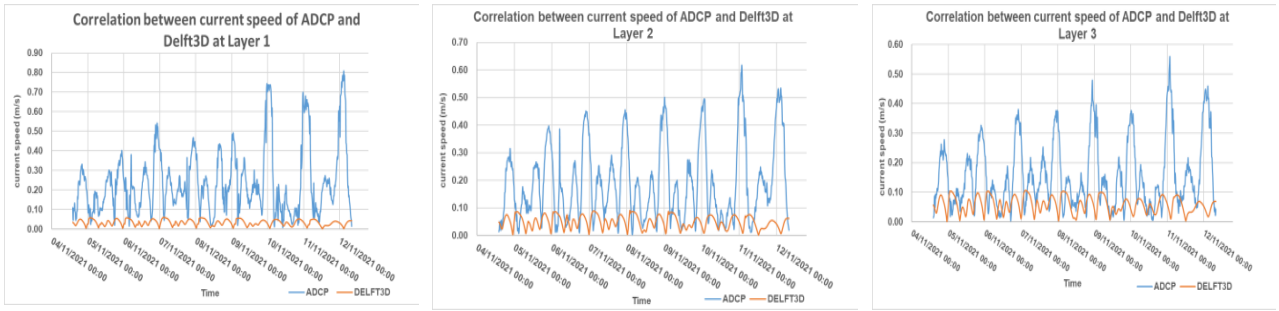


**Figure 17.** Comparison between current speed of ADCP and model on a 30km$^2$ domain.

## Conclusion

In this study, several accuracy calculation formulations were applied, namely: Skill, RMSE, NRMSE, and Correlation (R). Based on the water level validation of all simulation results, the error value is less than 10%, with a range of 5.3-9.60%. It means that the model has satisfactory performance in

reproducing nearshore hydrodynamics. The RMSE calculation value also shows that the input boundary condition TPXO 8.0 is better than TPXO 7.2 in the two-dimensional simulation around the Cisadane River. In addition, the Manning number was also applied as one of the sensitivity test parameters that abruptly affect modeling results. On two-dimensional simulation, the statistical value shows that manning number 0.045 produced the smallest error. Among all layers in three-dimensional models, the optimum current velocity (u-v components) correlation has been reached by L3 (bottom layer) towards primary data with a correlation of 0.797. Overall, three-dimensional hydrodynamics reached the best configuration in manning number 0.035 and domain size 10 km$^2$.

## Acknowledgement

The author thanked the Disaster Technology Program House Funding, Research Organization for Energy and Manufacture - National Research and Innovation Agency (BRIN) with the DIPA number 124.01.KB.6693.SDB.001.051.A, Research Centre for Hydrodynamics Technology- BRIN, BTIPDP's survey team, and all personnel in this program for supporting the implementation of this research activity. GRP, HHRS, HK, and RW as main contributors, contributed to make the entire model, including preparing the scenario, preprocessing, processing, post-processing, and analyzing the result, and GG revised the final draft.

## References

Abidin, H.Z., Andreas, H., Gumilar, I., Fukuda, Y., Pohan, Y.E. & Deguchi, T. 2011. Land Subsidence of Jakarta (Indonesia) and Its Relation with Urban Development. *Nat. Hazards,* 59: 1753-1771. https://doi.org/10.1007/s11069-011-9866-9

Bao, W.M., Zhang, X.Q. & Qu, S.M. 2009. Dynamic correction of roughness in the hydrodynamic model. *J. Hydrodynam.*, 21(2): 255-263. https://doi.org/10.1016/S1001-6058(08)60143-2

Bastidas, L.A., Knighton, J. & Kline, S.W. 2016. Parameter Sensitivity and Uncertainty Analysis for a Storm Surge and Wave Model. *Nat. Hazards Earth Syst. Sci.*, *16*(10): 2195–2210. https://doi.org/10.5194/nhess-16-2195-2016

Brakenhoff, L., Schrijvershof, R., Van der Werf, J., Grasmeijer, B., Ruessink, G. & Van der Vegt, M. 2020. From Ripples to Large-Scale Sand Transport: The Effects of Bedform-Related Roughness on Hydrodynamics and Sediment Transport Patterns in Delft3d. *J. Mar. Sci. Eng.*, *8*(11): p.892. https://doi.org/10.3390/jmse8110892.

Briere, C., Giardino, A. & Van der Werf, J. 2011. Morphological Modeling of Bar Dynamics with DELFT3d: The Quest for Optimal Free Parameter Settings Using an Automatic Calibration Technique. *Coast. Eng. Proc.*, 1(32): 1-12. https://doi.org/10.9753/icce.v32.sediment.60

Cea, L. & French, J.R., 2012. Bathymetric error estimation for the calibration and validation of estuarine hydrodynamic models. *Estuar. Coast. Shelf Sci.*, 100: 124-132. https://doi.org/10.1016/j.ecss.2012.01.004

Deltares. 2022. Delft3D-FLOW Simulation of Multi-Dimensional Hydrodynamic Flows and Transport Phenomena, *Including Sediments User Manual*.

Gao, L., Sun, H., Lin, T., Sui, J. & Ni, X. 2017. Metal Artifact Reduction for Dental Implants in Kilovoltage Computed Tomography Using Megavoltage Cone-Beam Computer Tomography. *J. Biomed. Eng.*, *34*(5): 730-737. https://doi.org/10.7507/1001-5515.201609071

Holt, T., Altaf, U., Mandli, K., Hadwiger, M., Dawson, C.N. & Hoteit, I. 2015. Visualizing Uncertainties in a Storm Surge Ensemble Data Assimilation and Forecasting System, *Nat. Hazards*, 77: 31–336. https://doi.org/10.1007/s11069-015-1596-y

Ihsan, Y. N. 2020. Marine Macro Debris Transport Based on Hydrodynamic Model Before and After Reclamation in Jakarta Bay, Indonesia. *Mal. J. Fund. Appl. Sci.*, *5*(2): 100-111. https://doi.org/10.37231/myjas.2020.5.2.241

Jasmin, H.H., Purba, N.P., Harahap, S.A., Pranowo, W.S., Syamsudin, M.L. & Faizala, I. 2019. The Model of Macro Debris Transport Before Reclamation and in Existing Condition in Jakarta Bay. *J. Ilmu Teknol. Kelaut. Tropis*, 11(1): 131-140. https://doi.org/10.29244/jitkt.v11i1.24777

Khoirunnisa, H., Wibowo, M., Hendriyono, W. & Wardani, K.S. 2021. The Hydrodynamics Condition of Water Operating Area for Flight Test Site Selection of N219 Amphibious Aircraft. *IOP Conf. Ser. Earth Environ. Sci*., 930(1): p012056. https://doi.org/10.1088/1755-1315/930/1/01 2056

Klement, A., Jaksik, O., Kodesova, R., Drabek, O. & Boruvka, L. 2013. Application of VNIR Diffuse

Reflectance Spectroscopy to Estimate Soil Organic Carbon Content, and Content of Different Forms of Iron and Manganese. *EGU General Assembly Conference Abstracts,* p. EGU2013-10846.

Koh, C.H., Khim, J.S., Araki, H., Yamanishi, H., Mogi, H. and Koga, K. 2006. Tidal resuspension of microphytobenthic chlorophyll a in a Nanaura mudflat, Saga, Ariake Sea, Japan: flood–ebb and spring–neap variations. *Mar. Ecol. Prog. Ser.*, 312: 85-100. https://doi.org/10.3354/mmeps312085

Mayo, T., Butler, T., Dawson, C. & Hoteit, I. 2014. Data Assimilation within The Advanced Circulation (ADCIRC) Modeling Framework for The Estimation of Manning's Friction Coefficient. *Ocean Model.*, *76*: 43–58. https://doi.org/10.1016/j.ocemod.2014.01.001

Molteni, F., Buizza, R., Palmer, T.N. & Petroliagis, T. 1996. The ECMWF ensemble prediction system: Methodology and validation. *Q. J. R. Meteorol. Soc.*, 122(529): 73-119. https://doi.org/10.1002/ qj.49712252905

Nugroho, A. & Magdalena, I. 2020. Hydrodynamic Model for Investigating the Impact of Reclamation Islands in Jakarta Bay to Mangrove Ecosystem in The Area. *AIP Conf. Proc.*, 2268(1): p.050003. https://doi.org/10.1063/5.0016899

Nuraghnia, A., Windupranata, W., Hakim, A.R. & Nusantara, C.A.D.S. 2021. Modeling of tide in the Java Sea coastal area between Jakarta and Cirebon, Indonesia: bathymetric data source and sensitivity tests due to bottom roughness and boundary condition. *IOP Conf. Ser. Earth Environ. Sci.,* 777(1): p.012034. https://doi.org/10.1088/1755-1315/777/1/0 12034

Octavianti, T. & Charles, K. 2018. Disaster Capitalism? Examining The Politicisation of Land Subsidence Crisis in Pushing Jakarta's Seawall Megaproject. *Water Altern.*, 11(2): 23-32.

Ormondt, M.V., Nederhoff, K. & van Dongeren, A. 2020. Delft Dashboard: a Quick Set-up Tool for Hydrodynamic Models. *J. Hydroinformatics*, 22(3): 510-527. https://doi.org/10.2166/hydro.2020.092

Parsapour-moghaddam, P., Rennie, C.D. & Slaney, J. 2018. Hydrodynamic Simulation of an Irregularly Meandering Gravel-Bed River: Comparison of MIKE 21 FM and Delft3D Flow models. *E3S Web Conf.*, 40: p.02004. https://doi.org/10.1051/e3sconf/20184002004

Pratama, M.B., Venugopal, V., Ajiwibowo, H., Ginting, J.W. & Novico, F. 2020. Modelling tidal flow hydrodynamics of Sunda Strait, Indonesia. *Ilmu Kelautan: Indonesian Journal of Marine Science*, 25(4): 165-172. https://doi.org/10.14710/ik.ijms.25.4. 165-172

Presidential Regulation. 2020. Appendix to Presidential Regulation (PERPRES) No. 18/ 2020 concerning the 2020-2024 National Medium Term Development Plan (LN.2020/NO.10, JDIH.SETKAB.GO.ID: 7 HLM.) Secretariat of the Republic of Indonesia.

Rautenbach, C., Barnes, M.A. & de Vos, M. 2019. Tidal Characteristics of South Africa. *Deep Sea Res. Part I Oceanogr. Res. Pap.,* 150: p.103079. https://doi.org/10.1016/j.dsr.2019.103079

Schober, P., Boer, C. & Schwarte, L.A. 2018. Correlation Coefficients: Appropriate Use and Interpretation. *Anesth. Analg.*, 126(5): 1763-1768. https://doi.org/10.1213/ANE.0000000000002864

Subsidence, D.T. 2015. Sinking Cities: An Integrated Approach Towards Solutions.http://publications.deltares.nl/Deltares142.pdf

Surya, M.Y., He, Z., Xia, Y. & Li, L. 2019. Impacts of sea level rise and river discharge on the hydrodynamics characteristics of Jakarta Bay (Indonesia). *Water*, 11(7): p.1384. https://doi.org/10.3390/w11071384

Symonds, A. M., Vijverberg, T., Post, S., Van Der Spek, B.J., Henrotte, J. & Sokolewicz, M. 2016. Comparison between Mike 21 FM, Delft3D and Delft3D FM flow models of western port bay, Australia. *Coast. Eng.,* 2: 1-12. https://doi.org/10.9753/icce.v35.currents.11

Technology Center of Ports Infrastructure and Coastal Dynamics (BTIPDP). 2021. Survey Report

Wahyudi, H.A.A., Haditiar, Y., Ikhwan, M., Wafdan, R., Setiawan, I., Muhammad, M., Sugianto, S. & Rizal, S. 2019. Numerical Study of Tides in the Bay of Sabang. *IOP Conf. Ser. Earth Environ. Sci*., 348(1): p.012096. https://doi.org/10.1088/1755-1315/ 348/1/012096

Walstra, D.J.R., Sutherland, J., Hall, L., Blogg. H. & Ormondt, M.V. 2001. Verification and Comparison of Two Hydrodynamic Area Models for an Inlet System. *Fourth Conference on*

*Coastal Dyn*., 01: 433-442. https://doi.org/ 10.1061/ 40566(2 60)44

Warner, J.C., Geyer, W.R. & Lerczak, J.A. 2005. Numerical modeling of an estuary: A comprehensive skill assessment. *J. Geophys. Res. Oceans*, 110(C5): p.23. https://doi.org/10. 1029/ 2004JC002691

Wibowo, M., Khoirunnisa, H., Wardhani, K. S. & Wijayanti, R. 2022. Pemodelan Pola Sedimentasi di Muara Cisadane untuk Mendukung Pengembangan Terpadu Pesisir Ibukota Negara. *J. Kelaut. Trop.*, 25(2): 179-190. https://doi.org/ 10.14710/jkt.v25i2.13732

Williams, J.J. & Esteves, L.S. 2017. Guidance on setup, calibration, and validation of hydrodynamic, wave, and sediment models for shelf seas and estuaries. *Adv. Civ. Eng*., 2017: 1-25. https://doi.org/10.1155/2017/5251902